Superconducting properties of noncentrosymmetric superconductor CaIrSi_{3} investigated by muon spin relaxation and rotation

Benjamin A. Frandsen, Sky C. Cheung, Tatsuo Goko, Lian Liu, Teresa Medina, Timothy S. J. Munsie, Graeme M. Luke, Peter J. Baker, Marco P. Jimenez S., Gaku Eguchi, Shingo Yonezawa, Yoshiteru Maeno, and Yasutomo J. Uemura

Phys. Rev. B **91**, 014511 — Published 23 January 2015

DOI: 10.1103/PhysRevB.91.014511

Superconducting properties of noncentrosymmetric superconductor $CaIrSi_3$ investigated by muon spin relaxation and rotation

Benjamin A. Frandsen,[1] Sky C. Cheung,[1] Tatsuo Goko,[2] Lian Liu,[1] Teresa Medina,[3] Timothy S. J. Munsie,[3] Graeme M. Luke,[3,4] Peter J. Baker,[5] Marco P. Jimenez S.,[6] G. Eguchi,[7] S. Yonezawa,[6] Yoshiteru Maeno,[6] and Yasutomo J. Uemura[1,*]

[1]*Department of Physics, Columbia University, New York, NY 10027, USA.*

[2]*Laboratory for Muon Spin Spectroscopy, Paul Scherrer Institut, CH-5232 Villigen PSI, Switzerland.*

[3]*Department of Physics and Astronomy, McMaster University, Hamilton, Ontario L8S 4M1, Canada.*

[4]*Canadian Institute for Advanced Research, Toronto, Ontario M5G 1Z8, Canada.*

[5]*ISIS Facility, STFC Rutherford Appleton Laboratory, Harwell Oxford, Oxfordshire OX11 0QX, United Kingdom*

[6]*Department of Physics, Kyoto University, Kyoto 606-8502, Japan.*

[7]*Department of Electronic Science and Engineering, Kyoto University, Kyoto 615-8510, Japan.*

Abstract

We have employed muon spin relaxation and rotation (μSR) to investigate the superconducting properties of the noncentrosymmetric superconductor $CaIrSi_3$. Measurements of single-crystal specimens confirm the development of a robust superconducting state below $T_c = 3.55 \pm 0.1$ K with a ground-state magnetic penetration depth of $\lambda_L = 288 \pm 10$ nm and a coherence length of $\xi = 28.8 \pm 0.1$ nm. The temperature evolution of the superfluid density indicates a nodeless superconducting gap structure dominated by an isotropic spin-singlet component in the dirty limit, with a carrier density of $n = (4.6 \pm 0.2) \times 10^{22}$ cm^{-3} as determined by Hall resistance measurements. We find no evidence of spontaneous time-reversal symmetry breaking in the superconducting state within an accuracy of 0.05 G. These observations suggest that the influence of any spin-triplet pairing component or multiple gap structure associated with noncentrosymmetric physics is very weak or entirely absent in $CaIrSi_3$.

I. INTRODUCTION

Noncentrosymmetric superconductors (NCSCs), whose crystal structures lack inversion symmetry, have been predicted to display a number of unusual properties in the superconducting state[1–5]. Without an inversion center, the familiar odd and even parity labels of spin-singlet and spin-triplet Cooper pairs, respectively, are no longer meaningful. Instead, the Cooper pair wavefunction takes the form of an admixture of spin-singlet and triplet components. In addition, an asymmetric spin-orbit interaction can lift the spin degeneracy of energy bands, splitting the Fermi surface into two. These features can give rise to novel behavior in NCSCs, stimulating significant theoretical and experimental interest over the past decade.

Bulk NCSCs that attracted attention in the early stages of this research field were primarily heavy-fermion compounds such as $CePt_3Si$,[6] $CeRhSi_3$,[7] CeIrSi3,[8] and UIr.[9] Evidence of unconventional superconductivity, such as anomalously large upper critical fields[6] and anisotropic gap structures[10,11], has indeed been observed in some of these materials. However, strong correlation effects and the proximity of magnetic order in the phase diagrams of these heavy-fermion materials makes it difficult to disentangle the influence of noncentrosymmetry from these other effects. For this reason, the recent discovery of nonmagnetic, non-f-electron NCSCs such as those with the general formula $AMSi_3$ (A = Ca, Sr, Ba; M = Co, Rh, Ir, Ni, Pd, Pt) is significant, since it offers the possibility of more directly probing the effects of noncentrosymmetry on superconductivity[12–14].

$CaIrSi_3$ is one of these recently discovered NCSCs[15]. It falls under space group $I4mm$ and has a superconducting critical temperature of $T_c = 3.6$ K, the highest known T_c for compounds with this crystal structure. A Rashba-type spin-orbit interaction splits the Fermi surface by a relatively large magnitude of $\sim$0.1-0.4 eV.[16] The results of initial characterization of polycrystalline samples, including magnetization, transport, and specific heat measurements, were generally consistent with conventional isotropic, fully gapped behavior[14,17], with only indirect hints of possible unconventional characteristics such as an unusual temperature dependence of the upper critical field[13]. The successful synthesis of single crystals of $CaIrSi_3$ has been important[16], since subtle features of unconventional superconductivity are often obscured in polycrystalline samples[18]. Studies of these single-crystal specimens have further revealed unusual magnetization behavior suggestive of anisotropic vortex pinning and possible multigap superconductivity, but with most other properties still well explained by conventional isotropic, fully-gapped superconductivity[16], leaving open the question of how significant noncentrosymmetric physics is for the superconducting properties of this material.

Muon spin relaxation and rotation (μSR) is an excellent tool to search for unconventional superconductivity. In particular, it allows a direct measurement of the superfluid density, which is intimately related to the superconducting gap structure. Indeed, calculations show that the parity mixing in NCSCs can lead to an unusual temperature dependence of the superfluid density[19], which has in fact been observed in the NCSC $CePt_3Si$.[11] Furthermore, μSR is an extremely sensitive probe of weak and disordered magnetism, and is therefore ideal for searching for the spontaneous time-reversal symmetry-breaking (TRSB) fields that have been found to arise in some unconventional superconductors such as the chiral p-wave superconductor Sr_2RuO_4 and the NCSC $LaNiC_2$.[20,21] For these reasons, μSR can be expected to shed light on the superconductivity of NCSCs.

In this paper, we present μSR measurements of $CaIrSi_3$ to investigate the superfluid density and possible existence of TRSB fields in the superconducting phase. Recently, similar μSR measurements were reported on a polycrystalline sample of $CaIrSi_3$,[22] but here we extend those results with measurements of high-quality single-crystal specimens. Our findings are consistent with the polycrystalline measurements, indicating a superconducting gap structure dominated by an isotropic spin-singlet component and no evidence for TRSB fields associated with noncentrosymmetric physics in this material. We also present Hall resistance measurements of the single-crystal specimens and confirm the dirty-limit nature of the superconductivity in $CaIrSi_3$.

II. METHODS

Small single crystal specimens of $CaIrSi_3$ with dimensions of roughly 0.5 mm $\times$ 0.5 mm $\times$ 0.5 mm were prepared according to methods described elsewhere[16]. Approximately 100 of these single crystals were mounted on a small silver plate with thermal grease and aligned such that the crystallographic c-axis of each crystallite was oriented normal to the silver plate. The basal ab-planes were not co-aligned.

Zero-field (ZF) μSR measurements were conducted at TRIUMF in Vancouver, Canada, using the Los Alamos Meson Physics Facility (LAMPF) spectrometer with a helium gas-flow cryostat with accessible temperatures down to 1.9 K, and at ISIS in Harwell, United Kingdom, using the MuSR spectrometer with an Oxford Instruments ^{3}He sorption cryostat capable of cooling to 0.3 K. ZF μSR is a highly sensitive probe of magnetism capable of routinely detecting static fields as small as 0.1 G. The technique involves implanting 100% spin-polarized muons into the sample, where the muons typically come to rest at an interstitial site. Each muon spin precesses around any local magnetic field present at the muon site until the muon spontaneously decays into a positron and two neutrinos

with a mean lifetime of 2.2 μs. Since the positron is emitted preferentially along the direction of the muon spin at the instant of decay, the total muon ensemble polarization is directly proportional to the difference between positron events recorded by opposing pairs of detectors, an experimental quantity known as the asymmetry $A(t)$. If no static magnetic order is present, $A(t)$ will be constant in time or relax very slowly due to random local fields arising from nuclear dipolar moments. In the presence of static magnetism, $A(t)$ will generally exhibit coherent precession if the magnetism is long-range ordered or increased damping if it is short-range ordered. Our measurements were configured such that the initial muon spin was oriented along the crystallographic c-axis.

We also performed transverse-field (TF) μSR measurements at TRIUMF, using both the gas-flow cryostat and a dilution refrigerator, extending the accessible temperature range down to 30 mK. TF μSR measurements operate under the same principles as ZF μSR but with the addition of an external magnetic field that is applied at the sample position in a direction perpendicular to the initial muon spin polarization. The muon spins then precess around the vector sum of the external field and any internal field at the muon site. Such a measurement can be extremely useful for studying type-II superconductors, since the muon spin depolarization rate due to the formation of the Abrikosov vortex lattice allows for direct determination of microscopic parameters such as the magnetic penetration depth λ_L and coherence length ξ, which can then be related to the superconducting gap symmetry and other important superconducting properties. Our measurements were configured such that the initial muon spin orientation was in the ab-plane with the external field directed along the c-axis.

The μSR analysis was performed in the time domain using the programs MSRFIT and MusrFit[23]. First-principles electronic structure calculations were computed with the full potential linearized augmented plane wave method, as described in a previous study[16]. Hall resistivity measurements down to 3 K were performed with a conventional four-probe technique in a commecial ^{4}He refrigerator (Quantum Design, PPMS).

III. RESULTS

We first present the TF μSR results. Two representative time spectra measured under an applied TF of 300 G are shown in Fig. 1, the top one taken at high temperature in the normal state and the bottom one at low temperature well inside the superconducting state. At high temperature, the asymmetry oscillates with very little damping, indicating that the internal field distribution is highly uniform. This is expected for TF μSR in the normal (paramagnetic) state. In stark contrast,

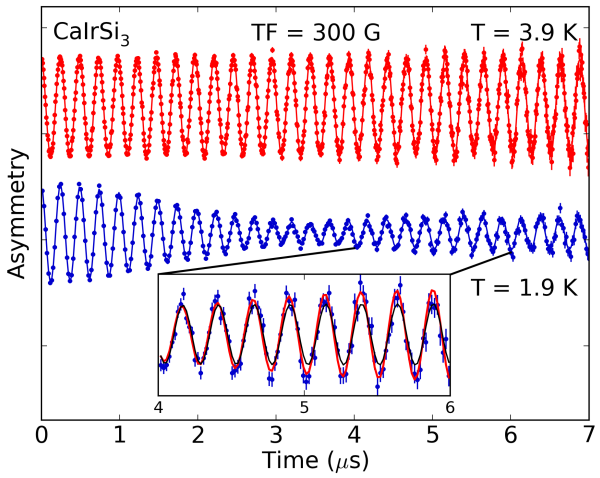

FIG. 1. (Color online) TF μSR time spectra measured above (top, red) and below (bottom, blue) the superconducting transition. The rapid damping in the superconducting state is characteristic of an ordered vortex lattice. Inset: Close-up view of the low-temperature spectrum from 4 μs to 6 μs, with fits of a simple Gaussian model (black) and a Ginzburg-Landau model (red) overlaid.

the spectrum measured in the superconducting state shows very pronounced damping, reflective of a much more inhomogeneous field distribution. The slight recovery of asymmetry after ~ 3.5 μs is due to beating between the signals from the sample-holder (26.5% weight) and the actual sample (73.5% weight), which are closely spaced in frequency. Inspection of the fast Fourier transforms (FFTs) of the time spectra, shown for several temperatures in the top panel of Fig. 2, reveals the anisotropic evolution of the high-temperature central peak near 4.0 MHz as the temperature is lowered well below T_c, with the FFTs at the lowest temperatures showing two distinct contributions from the sample (low-frequency side) and sample holder (high-frequency side). Important to note are the shift in frequency and the significant broadening of the sample component, both characteristic of the superconducting state. The lower panel shows the decomposition of the FFT at 1.9 K into an unshifted Gaussian peak arising from the sample holder (blue curve) and an anisotropic peak coming from the sample itself (red curve). Although the anisotropy of the sample component may not be immediately apparent from visual inspection of the raw FFT spectrum, it can be verified by comparing fit qualities for various models refined in the time domain, as described later. The anisotropic frequency distribution, which is equivalent to the internal field distribution, is caused by the formation of a well-ordered vortex lattice and is characterized by an extended tail on the high-frequency side of the peak. The expected field distribution from an ideal triangular vortex lattice[18] is given by the gray curve in the lower panel of Fig. 2. The observed field distribution is

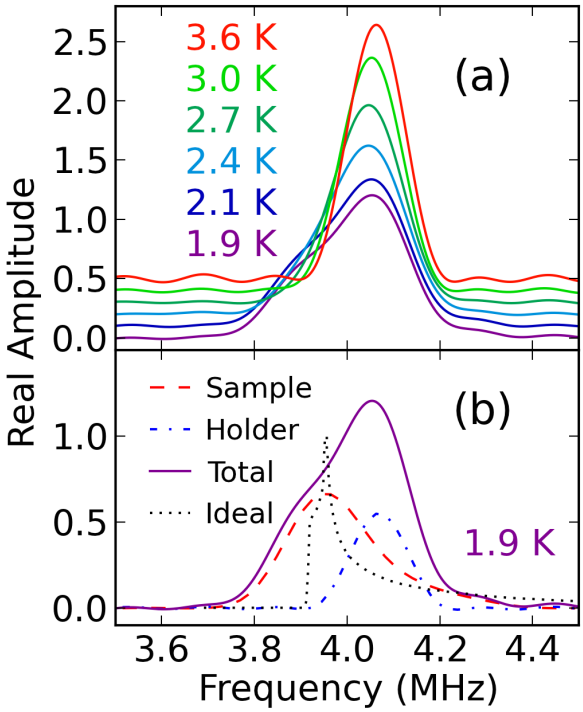

FIG. 2. (Color online) (a) Real amplitude of the Fourier transforms of the time spectra at various temperatures, offset vertically for clarity. The temperature list matches the order of the offset Fourier transforms from top to bottom. (b) Analysis of the Fourier transform at 1.9 K (purple solid curve) showing the Gaussian contribution from the sample holder (blue dashed-dotted curve), the anisotropic field distribution arising from the vortex lattice (red dashed curve), and the internal field distribution from an ideal triangular vortex lattice[18] (black dotted curve).

significantly broader due to the effects of disorder in the vortex lattice, randomly oriented nuclear dipolar moments, and the finite time window of the data, but nevertheless displays the general characteristics indicative of the vortex state.

The anisotropy of the frequency distribution, also called the μSR line shape, yields detailed information about the magnetic penetration depth λ_L and superconducting coherence length ξ, and can thus be used to gain microscopic insight into the superconducting properties of the material, such as the gap structure. For such a detailed study, single-crystal specimens are crucial, since the anisotropic line shape is typically broadened into an approximately Gaussian line shape for polycrystalline samples. For example, recent TF μSR measurements performed on a polycrystalline sample of $CaIrSi_3$ exhibit a purely Gaussian line shape with little to no hint of the anisotropy from the vortex lattice[22]. Lacking the information contained in the anisotropy of the line shape, it can be difficult to draw accurate conclusions. For instance, early μSR studies on polycrystal

and sintered pellet samples of cuprate systems suggested s-wave gap symmetry[24–26], and not until later measurements of high-quality single-crystal specimens was the actual d-wave gap symmetry verified[27,28].

To extract quantitative information about the superconducting state in $CaIrSi_3$, we have performed fits to all TF μSR time spectra with $T < 3.6$ K using two different models: a simple Gaussian model given by $A(t) \sim e^{-\sigma^2 t^2/2} \cos(\omega t + \phi)$, and a more sophisticated analytical Ginzburg-Landau (GL) model with a triangular Abrikosov lattice. In both cases, an additional temperature-independent Gaussian component representing the sample holder was included, and the free parameters were refined to minimize χ^2. The simple Gaussian model contains information about λ_L but not ξ, whereas the GL model provides sensitivity to both by allowing one to calculate the internal field distribution as a function of λ_L and ξ, or equivalently λ_L and the Ginzburg-Landau parameter $\kappa = \lambda_L/\xi$. This field distribution can subsequently be Fourier transformed into the time domain for comparison with the experimentally measured spectrum. We also included Gaussian-type broadening in the GL model to represent the effects of disorder in the vortex lattice and random fields from nuclear dipolar moments. Although the simple Gaussian model provided an adequate fit to the low-temperature spectra, the GL model fit the measured spectra significantly better, particularly at long times (see inset of Fig. 1). For comparison, the Gaussian model had $\chi^2 = 1.41$, while the GL model had $\chi^2 = 1.10$. This demonstrates that the data do in fact reflect an anisotropic field distribution. We therefore focus our discussion on the fits with the GL model.

After initially allowing both λ_L and κ to vary freely, we noticed that κ tended to converge to values between 8 and 11, although the exact value was correlated with λ_L. This is often the case when fitting a GL model to μSR data, so it is not uncommon to fix κ at a reasonable value for subsequent fits[29]. Applying this strategy, we fixed κ to 10 for the remaining refinements at all temperature points and allowed the other parameters to vary freely. We note that this value for κ is in very close agreement with $\kappa = 10.2$ determined from bulk measurements of specific heat and upper critical field on similarly prepared single-crystal specimens[16].

A representative fit to the TF μSR time spectrum is displayed as the solid blue line in the low-temperature spectrum of Fig. 1, showing the good agreement between the measured and calculated spectra. Using the refined values of the penetration depth, we plot as a function of temperature the quantity λ_L^{-2}, which is proportional to the superfluid density n_s (Fig. 3). In agreement with other μSR studies[22], a conventional isotropically gapped model describes the data well, as shown by the dashed black curve. Using this isotropic model, the refined critical temperature is $T_c = 3.55 \pm 0.1$ K and the refined penetration depth at zero temperature is $\lambda_L(0) = 288 \pm 10$ nm, corresponding well to

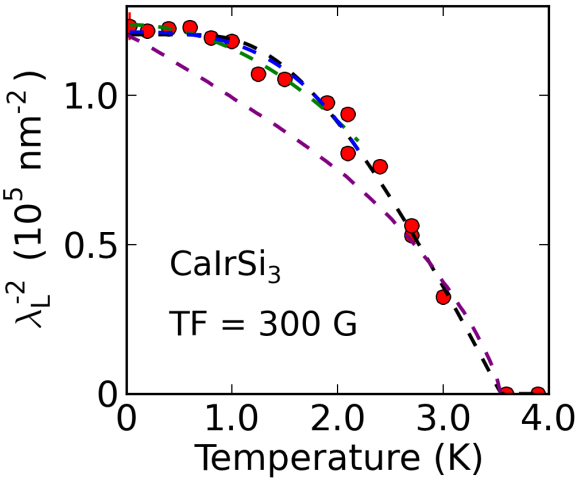

FIG. 3. (Color online) Temperature evolution of λ_L^{-2} as determined by fits to the μSR time spectra. Fitting an isotropically gapped model to the data results in the black dashed curve. The other dashed curves result from fits using a model with line nodes (purple), a T^2 power law (green), and a T^3 power law (blue). The T^2 and T^3 fits are only shown for the fitting range $T \leq 2.2$ K.

previous measurements[16]. With $\kappa = 10$, the corresponding coherence length is $\xi(0) = 28.8 \pm 0.1$ nm. These results are compared with other experimental studies of both polycrystalline and single-crystal $CaIrSi_3$ in Table I. The agreement between Refs. 13, 16, and the present work is particularly good. The discrepancies between the current study and the other μSR study[22] are most likely attributable to different specimen types (single-crystal vs. polycrystal) and fitting schemes. It is also known that certain synthesis routes can produce the impurity phase $CaIr_3Si_7$, which is likewise expected to affect the superconducting properties[13].

As an additional check for consistency, we also performed fits at all temperatures using the simple Gaussian model described earlier. We then fit an isotropically gapped model to the temperature dependence of the refined Gaussian relaxation rate (which is proportional to λ_L^{-2})[18], resulting in a best-fit relaxation rate of $\sigma_{\rm SC} = 0.838 \pm 0.015 \mu{\rm s}^{-1}$ at 0 K. To compare this Gaussian relaxation rate to the penetration depth, we use the relationship[30,31] $\sigma_{\rm SC}[\mu{\rm s}^{-1}] = (270/\lambda_L[{\rm nm}])^2$. This relationship has been justified through quantitative comparison of penetration depth measurements of cuprate superconductors YBCO, Bi2201, and other systems using μSR, microwave, and $H_{\rm c1}$ techniques. Using this conversion factor, the Gaussian relaxation rate corresponds to a penetration depth of approximately 295 nm, in very close agreement with the more accurate Ginzburg-Landau results.

We now move to the ZF μSR results, which are summarized in Fig. 4. Two representative spectra are displayed, one above $T_{\rm c}$ (red) and one below (black). They both show slow and nearly identical

TABLE I. Selected superconducting characteristics of $CaIrSi_3$. Where available, the estimated uncertainties of the reported values are provided.

	Polycrystal		Single Crystal	
	Ref. 13	Ref. 22	Ref. 16	Current Work
T_c (K)	3.6(1)	3.50(5)	3.55	3.55(10)
$\lambda_L(0)$ (nm)	280	150(7)	306	288(10)
$\xi(0)$ (nm)	34	—	30	28.8(1)
κ	8.3	—	10.2	10

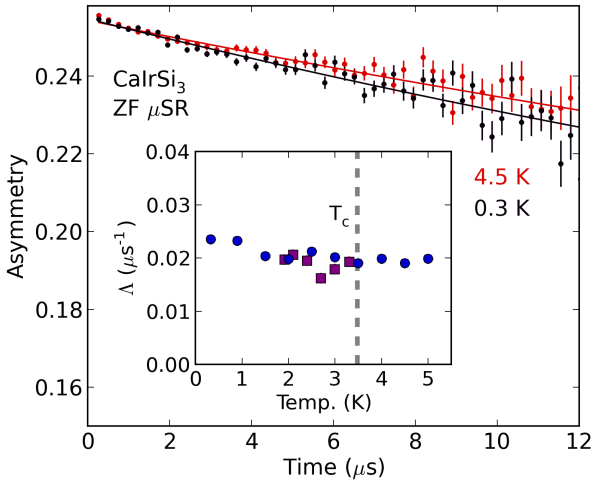

FIG. 4. (Color online) Zero-field muon spin relaxation measurements of $CaIrSi_3$. The red and black time spectra were measured above and below the superconducting transition, respectively. Inset: Temperature dependence of the refined exponential relaxation rate Λ. The blue circles correspond to data taken in a sorption cryostat at ISIS, the purple squares in a gas-flow cryostat at TRIUMF. The broken gray line shows the superconducting T_c. Estimated standard deviations of the refined parameters are smaller than the symbol size.

exponential relaxation. We performed fits to the ZF μSR spectra at several temperatures between 0.3 K and 4.5 K using the function

$$A(t) = a_{samp} \exp(-\Lambda t) + a_{bkg}, \tag{1}$$

where a_{samp} is the total initial asymmetry arising from muons landing in the sample, and the

constant a_{bkg} corresponds to muons landing in the silver sample holder, which is known to exhibit no relaxation. Since the sample size was small compared to the muon beam cross section at TRIUMF and even moreso at ISIS, we had to carefully consider the relative contributions of the sample and sample holder to the total signal. For the ZF data collected at TRIUMF, the sample and sample-holder contributions were accurately determined from the TF data, where they are well differentiated in precession frequency and relaxation rate. We found that 73.5% of the signal arises from the sample and 26.5% from the sample holder. Fixing this ratio, we then refined Eq. 1 to the ZF data, with the refined relaxation rate $\Lambda(t)$ shown as purple squares in the inset of Fig. 4.

The beam spot at ISIS is significantly larger than at TRIUMF, resulting in an increased background contribution. Since TF measurements at ISIS were not performed, we estimated the relative weight of the sample contribution to be 45% by fixing the initial sample asymmetry such that the refined high-temperature relaxation rate was comparable to that from the TRIUMF data. This refinement scheme allows for a consistent refinement of the relaxation rate at all temperatures and is expected to preserve the robustness of the temperature dependence, even if the absolute value of the relaxation rate may not be independently reliable. The refined relaxation rates from the ISIS data are shown as blue circles in the inset of Fig. 4. In both data sets, there is no systematic temperature-dependent trend evident in the refined relaxation rates. This agrees with previous ZF μSR measurements performed on a polycrystalline sample[22].

Finally, we report Hall resistivity measurements conducted on single-crystal specimens of $CaIrSi_3$ prepared in the same way as those used for the μSR measurements. After subtracting a minor longitudinal component of the resistivity, we plot in Fig. 5 the transverse Hall resistivity ρ_{yx} as a function of applied magnetic field measured at 3 K, 9 K, and 20 K. A linear fit was performed for the 3 K data, from which an electron carrier density of $n = (4.6 \pm 0.2) \times 10^{22}$ cm^{-3} was extracted. The carrier density has very little temperature dependence in the low-temperature regime. First-principles calculations with a semiclassical approximation[32] yield a carrier density of $n = 2.7 \times 10^{22}$ cm^{-3}, with a density of states at the Fermi level of $N(E_{\rm F}) = 1.94$ states/eV·f.u. These calculations are in relatively good agreement with the experimental value extracted from analysis of the Hall measurement, which assumes a simple one-band model. This suggests that the contributions of additional Fermi surfaces in the multiband scenario are quite minor, so we regard this experimental value for the carrier density as reasonable and useful for further analysis. Using this value, the effective mass of $m^* = 1.43\ m_{\rm e}$ determined by specific heat measurements[16], and assuming a simple Drude model and spherical Fermi surface, the mean free path ℓ can be calculated from the residual resistivity of 68 $\mu\Omega$ cm reported in Ref. 16, yielding $\ell = 1.5$ nm.

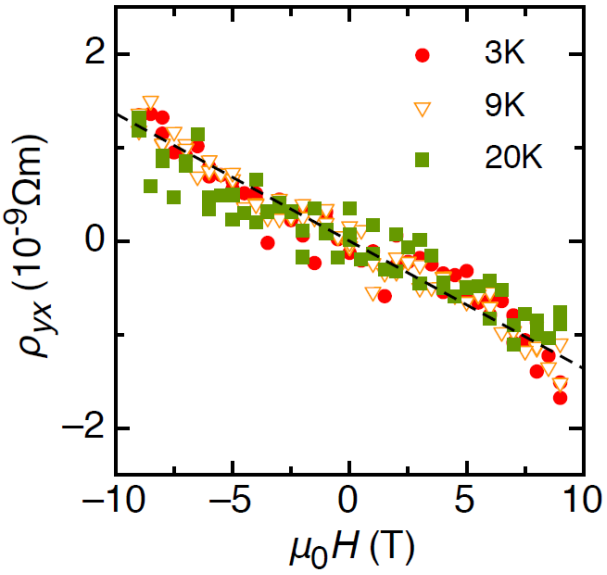

FIG. 5. (Color online) Hall resistivity ρ_{yx} as a function of applied magnetic field for three different temperatures. The dashed line indicates a linear fit to the 3 K data.

This relatively short mean free path is consistent with an average defect spacing arising from Ca vacancies on the order of a few percent, in agreement with energy-dispersive x-ray measurements. Comparing the mean free path to the superconducting coherence length determined from the GL fits described earlier, we find $\xi/\ell = 19 \gg 1$, indicating that $CaIrSi_3$ can be classified as a dirty-limit superconductor.

IV. DISCUSSION

$CaIrSi_3$ belongs to space group $I4mm$ with the point group C_{4v}, resulting in 5 irreducible representations that can be used to construct permissible superconducting pairing states[33]. The ZF- and TF-μSR measurements are sensitive to details of the superconducting gap function, including the presence of gap nodes and respect for time-reversal symmetry, and can therefore help determine which pairing state is realized in $CaIrSi_3$.

We first consider the ZF μSR results. The relaxation rate is temperature independent within the statistical uncertainty of the fits, suggesting that TRS is preserved in the superconducting state. To extract an upper limit for the magnitude of any TRSB fields, we note that to first order[34], the exponential relaxation rate Λ corresponds to a Lorentzian-type field distribution of width $\frac{3\Lambda}{4\gamma_\mu}$, where $\gamma_\mu = 0.085\ \mu s^{-1}G^{-1}$ is the muon gyromagnetic ratio. With the scatter in the data points of less than 0.005 μs^{-1}, we can set an upper limit of approximately 0.05 G as the characteristic

magnitude of any TRSB fields present in the material. For comparison, the chiral p-wave spin-triplet superconductor Sr_2RuO_4 exhibits TRSB fields of approximately 0.5 G.[20] Assuming then that the scatter in the refined relaxation rates is not significant, we conclude that TRS is preserved, which excludes the possibility of chiral E-type pairing states (e.g. $k_z k_x \pm \imath k_z k_y$) in the notation of Ref. 33.

Before discussing the TF-μSR measurements, we first comment on the implications of dirty-limit superconductivity in $CaIrSi_3$. Dirtiness results in increased scattering from impurities or defects, which in turn can be expected to "smear out" any otherwise sharp nodes from non-s-wave gap symmetries. This would affect the temperature dependence of the superfluid density and could tend to obscure any signatures of an unconventional pairing state in penetration depth measurements. In the past, the concern about smearing out the superfluid density in this way has generally focused on the use of polycrystalline rather than single-crystal specimens. However, even the present single-crystal sample of $CaIrSi_3$ is quite dirty and may therefore result in loss of information about the true pairing symmetry in penetration depth measurements. With this in mind, it seems notable that to our knowledge, all NCSCs showing clear deviations from conventional fully gapped penetration depth behavior, such as $CePt_3Si$ [Ref. 11], Li_2Pt_3B [Ref. 35], $LaNiC_2$ [Ref. 36], and $Mg_{10}Ir_{19}B_{16}$ [Ref. 37], are known to be in the clean limit or have relatively low residual resistivity approaching 0 K, indicative of a minor role played by defects or impurities. In the case of $Mg_{10}Ir_{19}B_{16}$, μSR measurements[38] performed on a specimen prepared by a method[39] resulting in a residual resistivity of 1400 $\mu\Omega$ cm found no hint of unconventional behavior in the penetration depth, whereas tunnel-diode oscillator measurements[37] on a cleaner sample with 100 $\mu\Omega$ cm residual resistivity[40] could not be explained by a single isotropic gap. In contrast, many NCSCs with penetration depth behavior fully consistent with conventional s-wave gap symmetry are known to be in the dirty limit or have substantial residual resistivity at low temperature, such as Mo_3Al_2C, $LaRhSi_3$, and $BaPtSi_3$. Reported information about TRSB, superconducting gap structure, residual resistivity, mean free path ℓ, and zero-temperature coherence length $\xi(0)$ for these and several other systems are listed in Table II. Considering these combined results, we suggest that caution must be used when attempting to determine the pairing symmetry from the penetration depth of NCSCs in the dirty limit, whether polycrystalline or single crystal, because signatures of unconventional pairing symmetries could be obscured. On the other hand, TRS measurements with ZF-μSR are expected to be only minimally affected by dirtiness.

Despite the possible limitations imposed by the intrinsically dirty nature of the superconductivity in $CaIrSi_3$, we proceed with a discussion of the TF-μSR results assuming that effects of dirtiness can be ignored. The TF-μSR data shown in Fig. 3 demonstrate that the superfluid density is

TABLE II. Presence of time-reversal symmetry breaking (TRSB) and unconventional superconducting gap structure (considered here to be anything that is not a single isotropic gap) in noncentrosymmetric superconductors in the clean vs. dirty limit. Materials known to be clean-limit superconductors are underlined; those that are dirty or unknown are not underlined.

Material	TRSB observed?	Unconventional gap?	RR* ($\mu\Omega$ cm)	ℓ (nm)	$\xi(0)$ (nm)
$\underline{CePt_3Si}$	No	Yes; TDO† (Ref. 11)	5.2 (Ref. 6)	80 (Ref. 6)	9 (Ref. 6)
$\underline{Li_2Pt_3B}$	No	Yes; TDO/μSR (Refs. 35,41)	28 (Ref. 41)	42 (Ref. 41)	14.5 (Ref. 41)
$\underline{LaNiC_2}$	Yes (Ref. 21)	Yes; TDO (Ref. 36)	6 (Ref. 42)	200 (Ref. 42)	26 (Ref. 42)
$Mg_{10}Ir_{19}B_{16}$	No (Ref. 38)	Yes; TDO (Ref. 37)	100 (Ref. 40)	—	—
Re_6Zr	Yes (Ref. 43)	No; μSR (Ref. 43)	—	—	—
SrPtAs	Yes (Ref. 44)	No; μSR (Ref. 44)	62 (Ref. 45)	—	38.7 (Ref. 45)
Mo_3Al_2C	No (Ref. 46)	No; μSR (Ref. 46)	125 (Ref. 47)	3.06 (Ref. 47)	4.6 (Ref. 47)
$LaRhSi_3$	No (Ref. 48)	No; μSR (Ref. 48)	1 (Ref. 48)	122 (Ref. 48)	344 (Ref. 48)
$BaPtSi_3$	No	No; μSR (Ref. 12)	6 (Ref. 12)	77 (Ref. 12)	99 (Ref. 12)
$CaIrSi_3$	No (current work)	No; μSR	68 (Ref. 16)	1.5	28.8

$*$ Residual resistivity

† Tunnel diode oscillator method

relatively temperature independent below about 1 K, suggesting fully gapped superconductivity. An anisotropic superconducting gap with line nodes as in NCSC $CePt_3Si$[11] would lead to a finite suppression of superfluid density as the temperature is raised slightly above 0 K. Such a situation is illustrated by the purple broken line in Fig. 3, which clearly disagrees with the observed temperature dependence of the superfluid density, allowing us to rule out this possibility. The absence of line nodes excludes pairing functions of type A_2, B_1, and B_2 in the notation of Ref. 33, leaving A_1 as the only pairing symmetry consistent with the μSR data. Furthermore, the singlet component must be dominant, since a dominant triplet component would lead to accidental line nodes[33] and is therefore inconsistent with the μSR data. This result agrees with bulk thermodynamic measurements performed on similar single crystals[16]. The TF data can be well described at all temperatures

below T_c with a single isotropic superconducting gap structure, as shown by the broken black line in Fig. 3. However, we cannot rule out the possibility of weak anisotropies arising from a small spin-triplet component. We also note that the low-temperature data ($T \leq 2$ K) can be reasonably well described by T^2 and T^3 power law fits (green and blue broken curves in Fig. 3, respectively), leaving open the possibility of point nodes or the special case of an equatorial line node[49] (which would require that the magnitudes of the spin-singlet and triplet components be exactly equal).

Other observations also support the conclusion that any spin-triplet component of the gap function, if present, is likely to be very small. The value of T_c does not differ very much among samples and the superconducting transition is reasonably sharp. If a spin-triplet component were dominant, T_c would be expected to be highly dependent on sample quality and would lead to a broad superconducting transition even in zero field. Moreover, the electronic specific heat C_e/T approaches zero at low temperature[16], whereas a significant spin-triplet component would be more likely to result in some residual density of states at very low temperature. These observations combined with the present μSR results strongly suggest that the pairing state of $CaIrSi_3$ is dominated by an isotropic spin-singlet component, even with the potential ambiguities introduced by the dirtiness of $CaIrSi_3$.

The rather conventional behavior of $CaIrSi_3$ observed in both TF- and ZF-μSR indicates that the noncentrosymmetric structure of this material does not result in a large spin-triplet pairing component or multiple gap structure measurable by μSR. We note that conventional superconductivity in NCSCs is not uncommon[50–53], despite the theoretical possibility of exotic behavior. It has been suggested that the presence of substantial electronic correlations is a necessary ingredient for appreciable spin-triplet pairing in NCSCs[54], which is one possible explanation for the apparent lack of unconventional behavior in the uncorrelated compound $CaIrSi_3$. On the other hand, other uncorrelated materials such as Li_2Pt_3B can exhibit spin-triplet pairing[35,55] and an anisotropic superconducting gap[56], leaving the role of electronic correlation an open question.

Finally, we offer one more comment regarding clean- versus dirty-limit superconductivity in $CaIrSi_3$. If the material were in the clean limit, the penetration depth could be calculated from the well-known relation

$$\lambda_{clean}(0) = \left(\frac{m^* c^2}{4\pi n e^2} \right)^{1/2}, \tag{2}$$

from which the dirty-limit penetration depth could be approximated as

$$\lambda_{dirty}(0) = \lambda_{clean}(0) \sqrt{1 + \xi/\ell}. \tag{3}$$

Substituting the measured values of n, m^*, ξ, and ℓ into these equations, we obtain $\lambda_{clean} = 29$ nm and $\lambda_{dirty} = 135$ nm. Although quantitative agreement is lacking, the measured value of $\lambda_L(0) =$

288 nm obtained via μSR strongly supports the dirty-limit nature of the superconductivity in $CaIrSi_3$. Given the high level of consistency among the experimental values of the penetration depth as seen in Table I, one might ask why the theoretically predicted value is substantially lower than the measured values. One possible source of disagreement is the approximate dirty-limit correction given in Eq. 3, which may not be quantitatively accurate. We suggest that the reevaluation of this commonly used correction factor would be a worthwhile theoretical endeavor.

V. CONCLUSION

We have presented TF- and ZF-μSR measurements of single-crystal specimens of $CaIrSi_3$ to gain insight into the superconducting properties of this material. The TF = 300 G data reveal a well-ordered Abrikosov vortex lattice in a bulk dirty-limit superconducting state possessing a gap structure that is dominated by an isotropic spin-singlet component, with a magnetic penetration depth of $\lambda_L = 288 \pm 10$ nm and a coherence length of $\xi = 28.8 \pm 0.1$ nm. The ZF data show a temperature-independent relaxation rate, indicating that TRS is preserved in the superconducting state. Taken together, these results suggest that the noncentrosymmetric structure of $CaIrSi_3$ does not lead to a large spin-triplet pairing component, multiple gap structure, or other unconventional behaviors detectable by μSR. We have also discussed the role of dirtiness in NCSCs and possible ensuing difficulties in detecting unconventional gap symmetries with μSR.

Acknowledgements

We thank Stephen Blundell for helpful discussions and assistance with the ISIS experiment. Work at Columbia University was supported by the U.S. National Science Foundation (NSF) via grant DMREF DMR-1436095 and the NSF PIRE program through grant OISE-0968226. B.F. acknowledges support from the NSF Graduate Research Fellowship under grant DGE11-44155. Additional support was provided by the grant KAKENHI (No. 22103002) from the Ministry of Education, Culture, Sports, Science and Technology (MEXT) of Japan. Research at McMaster University was supported by NSERC. Parts of this work were carried out at the CMMS TRIUMF facility and the STFC ISIS facility. G.E. acknowledges support from JSPS.

---

* tomo@lorentz.phys.columbia.edu

[1] V. M. Edelstein, Sov. Phys. JETP **68**, 1244 (1989).

[2] V. M. Edelstein, Physical Review Letters **75**, 2004 (1995).

[3] L.P. Gor'kov and E.I. Rashba, Physical Review Letters **87**, 037004 (2001).

[4] S.K. Yip, Physical Review B **65**, 144508 (2002).

[5] S. Fujimoto, J. Phys. Soc. Jpn **76**, 051008 (2007).

[6] E. Bauer, G. Hilscher, H. Michor, C. Paul, E. W. Scheidt, A. Gribanov, Y. Seropegin, H. Noël, M. Sigrist, and P. Rogl, Physical Review Letters **92**, 027003 (2004).

[7] N. Kimura, K. Ito, K. Saitoh, Y. Umeda, H. Aoki, and T. Terashima, Physical review letters **95**, 247004 (2005).

[8] I. Sugitani, Y. Okuda, H. Shishido, T. Yamada, A. Thamizhavel, E. Yamamoto, T. D. Matsuda, Y. Haga, T. Takeuchi, R. Settai, and Y. Ōnuki, J. Phys. Soc. Jpn **75**, 043703 (2006).

[9] T. Akazawa, H. Hidaka, H. Kotegawa, T. C. Kobayashi, T. Fujiwara, E. Yamamoto, Y. Haga, R. Settai, and Y. Ōnuki, J. Phys. Soc. Jpn **73**, 3129 (2004).

[10] N. Metoki, K. Kaneko, T. D. Matsuda, A. Galatanu, T. Takeuchi, S. Hashimoto, T. Ueda, Y. Settai, Ōnuki, and N. Bernhoeft, Journal of Physics: Condensed Matter **16**, L207 (2004).

[11] I. Bonalde, W. Brämer-Escamilla, and E. Bauer, Phys. Rev. Lett. **94**, 207002 (2005).

[12] E. Bauer, R.T. Khan, H. Michor, E. Royanian, A. Grytsiv, N. Melnychenko-Koblyuk, P. Rogl, D. Reith, R. Podloucky, E.-W. Scheidt, W. Wolf, and M. Marsman, Physical Review B **80**, 064504 (2009).

[13] G. Eguchi, D.C. Peets, M. Kriener, Y. Maeno, E. Nishibori, Y. Kumazawa, K. Banno, S. Maki, and H. Sawa, Physical Review B **83**, 024512 (2011).

[14] G. Eguchi, F. Kneidinger, L. Salamakha, S. Yonezawa, Y. Maeno, and E. Bauer, J. Phys. Soc. Jpn **81**, 074711 (2012).

[15] S. Oikawa, M. Nohara, and H. Takagi, Meeting Abstracts of the Physical Society of Japan **63 (2-3)**, 23pQC (2008).

[16] G. Eguchi, H. Wadati, T. Sugiyama, E. Ikenaga, S. Yonezawa, and Y. Maeno, Phys. Rev. B **86**, 184510 (2012).

[17] G. Eguchi, D. C. Peets, M. Kriener, S. Maki, E. Nishibori, H. Sawa, and Y. Maeno, Physica C: Superconductivity and its Applications **470**, S762 (2010).

[18] J. E. Sonier, J. H. Brewer, and R. F. Kiefl, Rev. Mod. Phys. **72**, 769 (2000).

[19] N. Hayashi, K. Wakabayashi, P.A. Frigeri, and M. Sigrist, Physical Review B **73**, 024504 (2006).

[20] G. Luke, Y. Fudamoto, K. Kojima, M. Larkin, J. Merrin, B. Nachumi, Y. Uemura, Y. Maeno, Z. Mao, Y. Mori, H. Nakamura, and M. Sigrist, Nature **394**, 558 (1998).

[21] A. D. Hillier, J. Quintanilla, and R. Cywinski, Physical Review Letters **102**, 117007 (2009).

[22] R. P. Singh, A. D. Hillier, D. Chowdhury, J. A. T. Barker, D. M. Paul, M. R. Lees, and G. Balakrishnan,

Phys. Rev. B **90**, 104504 (2014).

[23] A. Suter and B. Wojek, Physics Procedia **30**, 69 (2012), 12th International Conference on Muon Spin Rotation, Relaxation and Resonance (SR2011).

[24] D. R. Harshman, G. Aeppli, E. J. Ansaldo, B. Batlogg, J. H. Brewer, J. F. Carolan, R. J. Cava, M. Celio, A. C. D. Chaklader, W. N. Hardy, S. R. Kreitzman, G. M. Luke, D. R. Noakes, and M. Senba, Phys. Rev. B **36**, 2386 (1987).

[25] R. Kiefl, T. Riseman, G. Aeppli, E. Ansaldo, J. Carolan, R. Cava, W. Hardy, D. Harshman, N. Kaplan, J. Kempton, S. Kreitzman, G. Luke, B. Yang, and D. Williams, Physica C **153-155**, 757 (1988).

[26] Y. J. Uemura, V. J. Emery, A. R. Moodenbaugh, M. Suenaga, D. C. Johnston, A. J. Jacobson, J. T. Lewandowski, J. H. Brewer, R. F. Kiefl, S. R. Kreitzman, G. M. Luke, T. Riseman, C. E. Stronach, W. J. Kossler, J. R. Kempton, X. H. Yu, D. Opie, and H. E. Schone, Phys. Rev. B **38**, 909 (1988).

[27] J. E. Sonier, R. F. Kiefl, J. H. Brewer, D. A. Bonn, J. F. Carolan, K. H. Chow, P. Dosanjh, W. N. Hardy, R. Liang, W. A. MacFarlane, P. Mendels, G. D. Morris, T. M. Riseman, and J. W. Schneider, Phys. Rev. Lett. **72**, 744 (1994).

[28] G. Luke, Y. Fudamoto, K. Kojima, M. Larkin, J. Merrin, B. Nachumi, Y. Uemura, J. Sonier, T. Ito, K. Oka, M. de Andrade, M. Maple, and S. Uchida, Physica C **282-287**, 1465 (1997).

[29] T. J. Williams, A. A. Aczel, E. Baggio-Saitovitch, S. L. Bud'ko, P. C. Canfield, J. P. Carlo, T. Goko, J. Munevar, N. Ni, Y. J. Uemura, W. Yu, and G. M. Luke, Phys. Rev. B **80**, 094501 (2009).

[30] Y. Uemura, A. Keren, L. Le, G. Luke, B. Sternlieb, W. Wu, J. Brewer, R. Whetten, S. Huang, S. Lin, R. Kaner, F. Diederich, S. Donovan, G. Grüner, and K. Holczer, Nature **352**, 605 (1991).

[31] P. L. Russo, C. R. Wiebe, Y. J. Uemura, A. T. Savici, G. J. MacDougall, J. Rodriguez, G. M. Luke, N. Kaneko, H. Eisaki, M. Greven, O. P. Vajk, S. Ono, Y. Ando, K. Fujita, K. M. Kojima, and S. Uchida, Phys. Rev. B **75**, 054511 (2007).

[32] G. K. Madsen and D. J. Singh, Computer Phys. Comm **175**, 67 (2006).

[33] M. Sigrist, D. Agterberg, P. Frigeri, N. Hayashi, R. Kaur, A. Koga, I. Milat, K. Wakabayashi, and Y. Yanase, J. Magn. Magn. Mater. **310**, 536 (2007).

[34] Z. Deng, C. Jin, Q. Liu, X. Wang, J. Zhu, S. Feng, L. Chen, R. Yu, C. Arguello, T. Goko, F. Ning, J. Zhang, Y. Wang, A. Aczel, T. Munsie, T. Williams, G. Luke, T. Kakeshita, S. Uchida, W. Higemoto, T. Ito, B. Gu, S. Maekawa, G. Morris, and Y. Uemura, Nature Communications **2**, 422 (2011).

[35] H. Q. Yuan, D. F. Agterberg, N. Hayashi, P. Badica, D. Vandervelde, K. Togano, M. Sigrist, and M. B. Salamon, Phys. Rev. Lett. **97**, 017006 (2006).

[36] I. Bonalde, R. Ribeiro, K. Syu, H. Sung, and W. Lee, New J. Phys. **13**, 123022 (2011).

[37] I. Bonalde, R. L. Ribeiro, W. Brämer-Escamilla, G. Mu, and H. H. Wen, Phys. Rev. B **79**, 052506 (2009).

[38] A. A. Aczel, T. J. Williams, T. Goko, J. P. Carlo, W. Yu, Y. J. Uemura, T. Klimczuk, J. D. Thompson, R. J. Cava, and G. M. Luke, Physical Review B **82**, 024520 (2010).

[39] T. Klimczuk, Q. Xu, E. Morosan, J. D. Thompson, H. W. Zandbergen, and R. J. Cava, Phys. Rev. B **74**, 220502 (2006).

[40] G. Mu, H. Yang, and H.-H. Wen, Phys. Rev. B **82**, 052501 (2010).

[41] E. Häfliger, R. Khasanov, R. Lortz, A. Petrović, K. Togano, C. Baines, B. Graneli, and H. Keller, J. Supercond. Nov. Magn. **22**, 337 (2009).

[42] J. Chen, L. Jiao, J. Zhang, Y. Chen, L. Yang, M. Nicklas, F. Steglich, and H. Yuan, New J. Phys. **15**, 053005 (2013).

[43] R. P. Singh, A. D. Hillier, B. Mazidian, J. Quintanilla, J. F. Annett, D. M. Paul, G. Balakrishnan, and M. R. Lees, Phys. Rev. Lett. **112**, 107002 (2014).

[44] P. K. Biswas, H. Luetkens, T. Neupert, T. Stürzer, C. Baines, G. Pascua, A. P. Schnyder, M. H. Fischer, J. Goryo, M. R. Lees, H. Maeter, F. Brückner, H.-H. Klauss, M. Nicklas, P. J. Baker, A. D. Hillier, M. Sigrist, A. Amato, and D. Johrendt, Phys. Rev. B **87**, 180503 (2013).

[45] Y. Nishikubo, K. Kudo, and M. Nohara, J. Phys. Soc. Jpn **80**, 055002 (2011).

[46] E. Bauer, C. Sekine, U. Sai, P. Rogl, P. K. Biswas, and A. Amato, Phys. Rev. B **90**, 054522 (2014).

[47] E. Bauer, G. Rogl, X.-Q. Chen, R. T. Khan, H. Michor, G. Hilscher, E. Royanian, K. Kumagai, D. Z. Li, Y. Y. Li, R. Podloucky, and P. Rogl, Phys. Rev. B **82**, 064511 (2010).

[48] V. K. Anand, A. D. Hillier, D. T. Adroja, A. M. Strydom, H. Michor, K. A. McEwen, and B. D. Rainford, Phys. Rev. B **83**, 064522 (2011).

[49] D. Einzel, P. J. Hirschfeld, F. Gross, B. S. Chandrasekhar, K. Andres, H. R. Ott, J. Beuers, Z. Fisk, and J. L. Smith, Phys. Rev. Lett. **56**, 2513 (1986).

[50] K. Togano, P. Badica, Y. Nakamori, S. Orimo, H. Takeya, and K. Hirata, Physical review letters **93**, 247004 (2004).

[51] A. B. Karki, Y. M. Xiong, I. Vekhter, D. Browne, P. W. Adams, D. P. Young, K. R. Thomas, J. Y. Chan, H. Kim, and R. Prozorov, Phys. Rev. B **82**, 064512 (2010).

[52] A. B. Karki, Y. M. Xiong, N. Haldolaarachchige, S. Stadler, I. Vekhter, P. W. Adams, D. P. Young, W. A. Phelan, and J. Y. Chan, Phys. Rev. B **83**, 144525 (2011).

[53] P. K. Biswas, A. D. Hillier, M. R. Lees, and D. M. Paul, Physical Review B **85**, 134505 (2012).

[54] F. Kneidinger, L. Salamakha, E. Bauer, I. Zeiringer, P. Rogl, C. Blaas-Schenner, D. Reith, and R. Pod-

loucky, Phys. Rev. B **90**, 024504 (2014).

[55] M. Nishiyama, Y. Inada, and G.-q. Zheng, Phys. Rev. Lett. **98**, 047002 (2007).

[56] G. Eguchi, D. C. Peets, M. Kriener, S. Yonezawa, G. Bao, S. Harada, Y. Inada, G.-q. Zheng, and Y. Maeno, Phys. Rev. B **87**, 161203 (2013).